THE CONTRIBUTION OF SPIRAL ARMS TO THE THICK DISK ALONG THE HUBBLE SEQUENCE

L. A. Martinez-Medina ¹, B. Pichardo², A. Pérez-Villegas ³ & E. Moreno²

²Instituto de Astronomía, Universidad Nacional Autónoma de México, A.P. 70–264, 04510, México D.F., México; barbara@astro.unam.mx and

ABSTRACT

The first mechanism invoked to explain the existence of the thick disk in the Milky Way Galaxy, were the spiral arms. Up-to-date work summon several other possibilities that together seem to better explain this component of our Galaxy. All these processes must affect differently in distinct types of galaxies, but the contribution of each one has not been straightforward to quantify. In this work, we present a first comprehensive study of the effect of the spiral arms in the formation of thick disks, as going from early to late type disk galaxies, in an attempt to characterize and quantify this specific mechanism in galactic potentials. To this purpose, we perform numerical simulations of test particles in a three-dimensional spiral galaxy potential of normal spiral galaxies (from early to late types). By varying the parameters of the spiral arms we found that the vertical heating of the stellar disk becomes very important in some cases, and strongly depends on the galaxy morphology, pitch angle, arms mass and its pattern speed. The later the galaxy type, the larger is the effect on the disk heating. This study shows that the physical mechanism causing the vertical heating is different from simple resonant excitation. The spiral pattern induce chaotic behavior not linked necessarily to resonances but to direct scattering of disk stars, which leads to an increase of the velocity dispersion. We applied this study to the specific example of the Milky Way Galaxy, for which we have also added an experiment that includes the Galactic bar. From this study we deduce that the effect of spiral arms of a Milky-Way-like potential, on the dynamical vertical heating of the disk is negligible, unlike later galactic potentials for disks.

Keywords: galaxies: evolution — galaxies: kinematics and dynamics — galaxies: spiral — galaxies: structure

1. INTRODUCTION

Simulations of galaxy formation are coming to point where detailed processes of galaxies have never been explored before in detail, such as random and rotational velocities can be better studied and understood (Scannapieco et al. 2011). Details on disk potentials can be probed and compared with observations, and we are now able to shed some light on evolution of galaxies starting now on small scale stellar motions.

Dynamical heating of the Milky Way disk has now been known for over 60 years, mainly through observations in the solar vicinity. From those observations we learnt that stellar random motions correlate nicely with their ages known as the age- σ relation (Wielen 1977; Binney et al. 2000). In particular, in the case of the Milky Way disk, it is known that the radial velocity dispersion is twice as much as the vertical dispersion and that the radial scale length of the thick disk is much shorter than that of the thin disk (Bensby et al. 2011).

Recent studies also show that many, if not all, edgeon spiral galaxies appear to host dual disk systems (Gerssen & Shapiro Griffin 2012; van der Kruit & Searle 1981), a younger, dynamically colder and thinner component: the thin disk and at least one older component, (mainly) stellar, dynamically hotter and thicker component: the thick disk (Yoachim & Dalcanton 2006; Yoachim & Dalcanton 2008; Comerón et al. 2011).

It is still not straightforward to dilucidate the

mechanism responsible for the vertical heating of the disk from observations, specially since more likely it might be rather a combination of several possibil-Among the mechanisms proposed there are ities. some external to the disk such as hits by satellite galaxies or minor mergers (Huang & Carlberg 1997; Velazquez & White 1999; Benson et al. 2004; Font et al. 2001; Quinn et al. 1993; Villalobos & Helmi 2008; Di Matteo et al. 2011); scattering by dark halo objects or globular clusters (Vande Putte et al. 2009; Hänninen & Flynn 2002). And some of internal origin, such as, dynamical heating by direct encounters with giant molecular clouds (Carlberg 1987; Villumsen 1983; Lacey & Ostriker 1985; Lacey 1984; Spitzer & Schwarzrchild 1951; Inoue & Saitoh heating by encounters with the potential produced by long-lasting spiral arms (Faure et al. 2014) or irregular and transient spiral structure (Minchev & Quillen 2006; Fuchs 2001; Jenkins & Binney 1990; Barbanis & Woltjer 1967); perturbations from stellar bars (Saha, Tseng & Taam 2010); dissolution of young stellar clusters (Kroupa 2002); or during an intense star formation phase in a period of intense accretion very early in the history of the Galaxy (Snaith et al. 2014).

Because of the nature of these theories, the effects are dependent on galaxy morphology, particularly the intrinsic mechanisms such as bars and spiral arms. Therefore,

Departamento de Física, Centro de Investigación y de Estudios Avanzados del IPN, A.P. 14-740, 07000 México D.F., México; lmedina@fis.cinvestav.mx

³ Centro de Radioastronomía y Astrofísica, Universidad Nacional Autónoma de México, Apartado Postal 3–72, 58090 Morelia, Michoacán, México; mperez@astro.unam.mx

to deeply understand secular evolution of disk galaxies, it is critical to study dynamical heating in a good sample of different disk galaxy types. Finally, from the point of view of observations, the radial heating agent seems to vary exactly as expected if the agent were the spiral arms, which provides a good chance that the spiral structure has at least an important role as a heating mechanism in the plane of galactic disks (Gerssen & Shapiro Griffin 2012). The importance and influence of spiral arms, and even their very same nature is still under debate, there is no straightforward observational prove yet of their effect on stars, however it is nowadays considered to have a key role on large-scale galactic dynamics (Sellwood 2013), for a review, (Roskar et al. 2012; Minchev et al. 2012; Lépine et al. 2011; Quillen et al. 2011; Antoja et al. 2009). One plausible observational example are the stellar features seen in the velocity space, known as "moving groups" (Proctor 1869; Eggen 1959, 1977, 1990, 1996a,b; Wilson et al. 1923; Roman 1949; Soderblom & Mayor 1993; Majewski 1994; 1996); these structures might become the first clear, undirect though, evidence of the effect of the spiral arms (Chereul et al. 1998, 1999; Dehnen 1998; Famaey et al. 2005, 2008; Antoja et al. 2012; Pompéia et al. 2011). Of course, the spiral arms are not the only nor the prefered mechanism to explain moving groups, the galactic bar is other possibility.

In this work we focus on the very first proposal to explain the vertical heating (Wielen 1977), disregarded at some point in the history because of their negligible effect on the Milky Way disk: the dynamical heating by effect of the spiral arms. We attempt to isolate and quantify the contribution of the spiral arms to the disk heating of galaxies. We performed numerical simulations of test particles in a three-dimensional galactic potential that models spiral arms (Pichardo et al. 2003), adjusted to simulate spiral galaxies, from early to late types (Pérez-Villegas et al. 2012, 2013). We produced a set-up with relaxed initial conditions for a stellar disk. Finally we calculated the effect on the vertical heating of the stellar disk produced by the nonaxisymmetric large scale structures. We have included a preliminary study on a self-gravitating potential, known as PERLAS model (Pichardo et al. 2003, 2004) for the Milky Way Galaxy, that includes the spiral arms and the galactic bar.

This paper is organized as follows. The galactic models, initial conditions and methodology are described in Section 2. The role of each one of the parameters of the model is studied with detail in Section 3, where we present calculations of dispersion velocity, the velocity ellipsoid, time evolution for spiral galaxies from early to late types, and an application to the Milky Way Galaxy. Finally, in Section 4, we present our conclusions.

2. METHODOLOGY AND NUMERICAL IMPLEMENTATION

The effect of the spiral arms over the stellar disk has been studied profusely in either N-body simulations (Sellwood & Binney 2002; Roskar et al. 2012, 2013; Kawata et al. 2014) or with spiral patterns treated as perturbations to the axisymmetric background and modelling it as a density wave (De Simone et al. 2004; Minchev & Quillen 2006; Faure et al. 2014).

In N-body simulations, although self-consistent, it is not plausible to adjust a given specific galaxy, or

to isolate the effect for example, of the arms or establish in detail the role that each one of the parameters that characterize the spiral pattern play over the vertical heating of the disk. On the other hand, when treated as steady spirals exerted as a perturbation to the axisymmetric potential, according to the hypothesis of Lin & Shu (1969), the heating is minimum and linked only to the resonant regions of the spirals (Lynden-Bell & Kalnajs 1972; De Simone et al. 2004), being more efficient in the radial direction (Sellwood & Carlberg 1984; Minchey & Quillen 2006).

Here we use spiral arms that although steady, are very different in nature to the typically and widely employed in literature. The gravitational potential due to the spiral pattern is not a simple perturbation but is rather based on a mass density distribution. With this model of spiral arms our studies on the vertical heating of the disk contrast in general with the density wave approach (except of course, for really small spiral arm masses and pitch angles).

For the orbital study we employed then threedimensional galactic potentials to model normal spiral galaxies (Sa, Sb and Sc). The motion equations are solved in the non-inertial reference system of the spiral arms and in Cartesian coordinates (x', y', z'). The orbits are integrated for 5 Gyr with a Bulirsh-Stoer algorithm (Press et al. 1992), with a conservation of the Jacobi constant approximately up to 10^{-12} . The disk heating is computed through the measure of the velocity dispersion at different times.

2.1. Models for Normal Spiral Galaxies

The models include an axisymmetric component (bulge, massive halo and disk), as the background potential, formed by a Miyamoto & Nagai (1975) disk and bulge, and a massive halo (Allen & Santillán 1991). The parameters used to model normal spiral galaxies (Sa, Sb and Sc) are presented in Table 1 (compiled by Pérez-Villegas et al. (2013)).

Superposed to the axisymmetric components, for the spiral arms potential, we employed a bisymmetric selfgravitating three-dimensional potential, based on a density distribution, called PERLAS model (Pichardo et al. 2003). This potential consists of individual inhomogeneous oblate spheroids superposed along a logarithmic spiral locus (Roberts, Huntley & van Albada 1979). Each spheroid has a similar mass distribution, i.e., surfaces of equal density are concentric spheroids of constant semiaxis ratio. The model considers a linear fall in density within each spheroid. The minor and major semiaxes of each oblate spheroid are 0.5 and 1.0 kpc, respectively (this gives a width of the spiral arms of 2 kpc and height of 0.5 kpc from the disk plane) and the separation among the spheroid centers along the spiral locus is 0.5 kpc. The superposition of the spheroids begins and ends, in the ILR and CR, respectively. The density falls exponentially along the spiral arm, where the radial scale length of the galactic disk is used (depending on morphological type, see Table 1).

The mass assigned to build the spiral pattern is subtracted from the disk mass to keep the given model invariable in mass. PERLAS is a more realistic potential since it is based on a density distribution and considers the force exerted by the whole spiral structure, obtain-

Parameter	Value			Reference
	Sa	Sb	Sc	
	Axisy	immetric	Components	
M_B / M_D	0.9	0.4	0.2	1,2
M_D / M_H^{-1}	0.07	0.09	0.1	2,3
Rot. Velocity $(km s^{-1})$	320	250	170	4
$(V_D/V_{Rot})_{2R_h}$	0.51	0.65	0.70	
$M_D (10^{11} M_{\odot})$	1.28	1.21	0.51	3
$M_B (10^{11} M_{\odot})$	1.16	0.44	0.10	M_B/M_D based
$M_H (10^{11} M_{\odot})$	16.4	12.5	4.8	M_D/M_H based
Disk scale-length (kpc)	7	5	3	1,3
$b_1^2 \text{ (kpc)}$	2.5	1.7	1.0	
$a_2 \stackrel{2}{\sim} (kpc)$	7.0	5.0	5.3178	
$b_2^2 (kpc)$	1.5	1.0	0.25	
a ₃ ² (kpc)	18.0	16.0	12.0	
		Spiral		
locus		Logari		5,9,10
arms number		2	=	6
pitch angle (°)	8-40	9-45	10-60	4,7
M_{sp}/M_D	_	1-5		9
scale-length (kpc)	7	5	3	disk based
$\Omega_{sp} \; ({\rm km \; s^{-1} \; kpc^{-1}})$	-30	-25	-20	5,8
ILR position (kpc)	3.0	2.29	2.03	
CR position (kpc)	10.6	11.14	8.63	
inner limit (kpc)	3.0	2.29	2.03	\sim ILR position based
outer limit (kpc)	10.6	11.14	8.63	~CR position based

Table 1
Parameters of the Galactic Models

References. — (1) Weinzirl et al. 2009; (2) Block et al. 2002; (3) Pizagno et al. 2005; (4) Brosche 1971; Ma et al. 2000; Sofue & Rubin 2001; (5) Grosbøl & Patsis 1998; (6) Drimmel et al. 2000; Grosbøl et al. 2002; Elmegreen & Elmegreen 2014; (7) Kennicutt 1981; (8) Patsis et al. 1991; Grosbøl & Dottori 2009; Egusa et al. 2009; Fathi et al. 2009; Gerhard 2011; (9) Pichardo et al. 2003; (10) Seigar & James 1998; Seigar et al. 2006;

ing a more detailed shape for the gravitational potential, unlike a two-dimensional local arm such as the tight winding approximation (TWA) represented for a simple cosine function.

Spiral arms nature is a matter of discussion nowadays, particularly their long-lasting or transient nature. We have performed experiments with constant, transient, gradual and sudden presence of the spiral arms. Although the growth rate is an unknown parameter in galaxies, we have considered different cases to test. On one hand we produce a set of experiments where the total mass of the spiral arms is introduced at once $(t=0~{\rm Gyr})$. The second set of experiments, inserts the spiral arms mass linearly in a timelapse of 1 Gyr. And a third set of experiments for which the spiral arms are simulated as transient, they vanish and grow with a given periodicity.

2.2. Initial Conditions and Equilibrium of a Stellar Disk

The initial conditions set-up follows the Miyamoto-Nagai density profile we are imposing. This to avoid transient effects induced by differences between the initial particle distribution and the imposed disk potential. In this manner, the initial condition for the stellar disk is given by

$$\rho_{MN} = \frac{b_2^2 M_d}{4\pi} \frac{a_2 R^2 + (a_2 + 3\sqrt{z^2 + b_2^2})(a_2 + \sqrt{z^2 + b_2^2})^2}{(R^2 + (a_2 + \sqrt{z^2 + b_2^2})^2)^{5/2} (z^2 + b_2^2)^{3/2}},$$
(1)

where M_d is the mass of the galaxy disk, a_2 and b_2 are the radial and vertical scale-length, respectively. This three parameters span a range of values in our simulations in order to capture different galaxy morphologies and kind of spiral arms.

To distribute the particles according to the Miyamoto-Nagai density law we solved equation (1) with a root finder method. This is done by expressing the density $\rho(R,z)$ in terms of the ratios $\rho(R,0)/\rho(0,0)$ and $\rho(R,z)/\rho(R,0)$, which provides us an equation for R and z in terms of the density. The value of these ratios ranges from 0 to 1, therefore we can explore all the possible values of the density with a random function and solve it for R and z.

To assign velocities to the particles we follow the strategy proposed by Hernquist (1993) where velocities are distributed by an approximation using moments of the collisionless Boltzmann equation plus the epicycle approach.

Thus we proceeded as follow: once the density profile has been established, it is necessary to obtain the rotation velocity. This can be derived from Φ , the grav-

 $^{^{1}}$ Up to 100 kpc halo radius.

² b₁, a₂, b₂, and a₃ are scale lengths.

itational potential of the model

$$\Omega_c(R) = \left(\frac{1}{R} \frac{\partial \Phi}{\partial R}\right)^{1/2} \tag{2}$$

and $v_c = R\Omega_c(R)$, so the circular velocity is given by

$$v_c(R) = \left(R\frac{\partial\Phi}{\partial R}\right)^{1/2}.$$
 (3)

Once known Ω_c at any radii we obtain

$$\kappa = \left(4\Omega_c^2 + R \frac{d\Omega_c^2}{dR}\right)^{1/2},\tag{4}$$

known as the epicyclic frequency, necessary to calculate the velocity dispersion at R and to correct for the asymmetric drift.

To achieve the requirement for the stellar disk to be in equilibrium, it is necessary to introduce a given dispersion in the velocity as a function of R. The velocity dispersions in the three polar coordinates are

$$\sigma_R = 3.358 \frac{\Sigma(R)Q}{\kappa} \tag{5}$$

$$\sigma_{\phi} = \frac{1}{2} \frac{\sigma_R \kappa}{\Omega_c} \tag{6}$$

$$\sigma_z = \sqrt{\pi G \Sigma b_2},\tag{7}$$

where κ is the epicyclic frequency, $\Sigma(R)$ the surface density, b_2 is the vertical scale-length of the disk, and Q is the known Toomre parameter. According to Toomre (1964), local stability requires Q>1, we choose Q=1.1 and found this value to be sufficient for the three galaxy types. In this way the velocity dispersion depends on the mass of the components that form each galaxy.

The asymmetric drift correction is defined as

$$\langle v_{\phi} \rangle^2 = v_c^2 - \sigma_{\phi}^2 - \sigma_R^2 \left(-1 - 2 \frac{R}{\Sigma} \frac{\partial \Sigma}{\partial R} \right),$$
 (8)

is a correction that has to be implemented in the set up for the initial conditions given the fact that stellar orbits are not in general in circular orbits, instead, orbits follow epicycles around a guiding point at the position of the circular orbit and these epicycles are characterized by the epicyclic frequency κ .

Finally the particles are distributed in the velocity space as

$$v_{\phi} = \langle v_{\phi} \rangle \pm x \sigma_{\phi}$$

$$v_{R} = \langle v_{R} \rangle \pm x \sigma_{R}$$

$$v_{z} = \langle v_{z} \rangle \pm x \sigma_{z}$$
(9)

where x is a random number between 0 and 1, $\langle v_{\phi} \rangle$ is given by Eq. (8) and the average radial and vertical velocities are taken as $\langle v_R \rangle = \langle v_z \rangle = 0$.

2.3. Dispersion analysis

The disk heating is often referred as the increase in the velocity dispersion over the lifetime of a star. Any disk thickening is then related to an increase in the vertical velocity dispersion of the disk stars. In this paper we analyze the spiral arms effects on the stellar disk, based on the study of the vertical velocity dispersion and its dependence with the parameters that characterize the spiral pattern.

The vertical velocity dispersion σ_z , is then calculated in the simulations by dividing the plane z=0 into 1 kpc bins and computing, as usual, the squared root of the averaged squared vertical velocity for all the particles that fall into a given bin. This provide us the vertical velocity dispersion as a function of R. In order to establish the contribution of the spiral arms to the disk thickness we also compute σ_z as a function of time by measuring the velocity dispersion at a fixed radius R for every time code unit (in this case, every 100 Myr across 5 Gyr in the simulation).

2.4. Control Simulations: Testing the Initial Conditions Equilibrium

As described in section 2.2, the first goal is to build an initial stellar disk in equilibrium to be sure that any change seen in radial and vertical velocity dispersion is strictly due to the interaction of the spiral arms with the stellar disk and not originated by a spurious non-relaxed initial condition set-up.

For this test a control simulation was produced with only the axisymmetric components for the potential model. Stars are run by 5 Gyr, for all galaxy types. Figure 1 shows σ_z as a function of R at different stages in the temporal evolution for an Sa, Sb, and Sc galaxy.

From the figure it is clear that the vertical velocity dispersion do not evolve or deviate from the initial dispersion, as expected for a disk in equilibrium with the axisymmetric potential.

3. RESULTS

We present in this section a set of controlled experiments to study the dynamical heating of disks on spiral galaxies considering the spiral arms as the driver. The general purpose is to shed some light on the relative importance of these large-scale structures to other sources of dynamical heating in different morphological types. The experiments include studies of different structural and dynamical parameters of the spiral arms such as, different pitch angles, total spiral arms masses, angular speeds, transient, and one final case modeling the Milky Way Galaxy (with preliminary results that will be better developed in a future work).

3.1. Dependence of the disk heating induced by spiral arms with galaxy morphology

Spiral galaxies present a wide variety on morphological types, from massive bulge-dominated galaxies to practically bulgeless disks, spanning a wide range of values for the parameters that characterize different galaxy types.

Figure 2 shows the velocity dispersion, σ_z , as a function of the galactocentric radius, R, at different times in the simulation for our galactic models: Sa, Sb and Sc (introduced in Section 2). For these three simulations

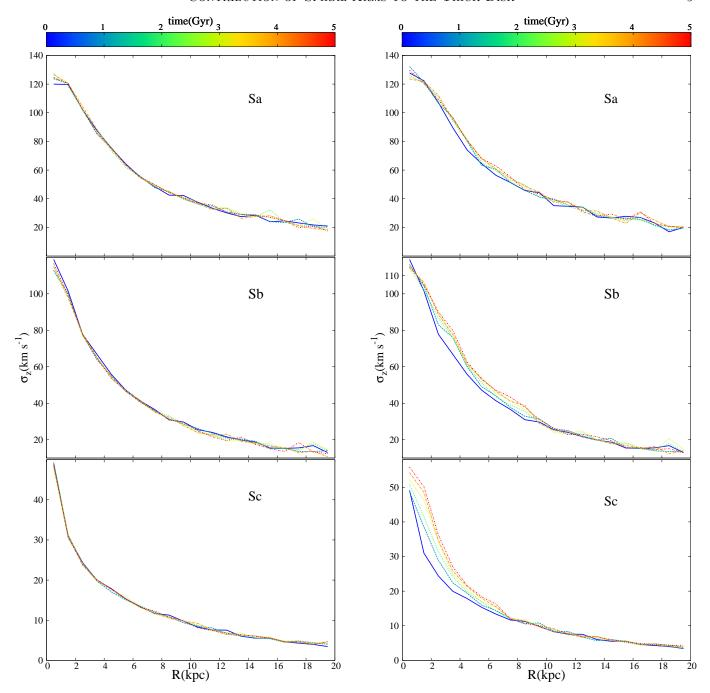


Figure 1. Test for the initial conditions equilibrium: velocity dispersion of the stellar disk in the axisymmetric potential only, as a function of R, along 5 Gyr time evolution for each galaxy type.

the mass of the spiral arms, M_{arms} , is 5% of the total disk mass with a Pitch angle of 40° for the Sa galaxy, 45° for the Sb galaxy, and 40° for the Sc galaxy. For these experiments we have employed the largest spiral arms masses and pitch angles, for plausible (non-fully chaotic) galactic models, to identify clearly spiral arms effects, if any. The three plots show a distinct increase in the vertical velocity dispersion caused by the spiral arms. Also from figure 2 it is clear that the change in σ_z with respect to the initial dispersion is smaller for the Sa galaxy and grows with the morphological type, being much larger for the Sc galaxy model.

Figure 2. As in Figure 1, but including now the spiral arms contribution to the potential. The vertical velocity dispersion is plotted as a function of R for 5 Gyr time evolution.

The dependence of the effect of the spiral arms with the morphology is such that for an Sc galaxy the effect is evident in the spatial distribution of the stellar disk particles. Figure 3 shows the x-z projection of the stellar distribution plotted at $t=0,\ t=2.5\,\mathrm{Gyr},$ and $t=5\,\mathrm{Gyr}.$

Also, a thickening of the disk is discernible during the orbital evolution when comparing with the initial distribution

The thickness can be quantified by computing the root mean square of the coordinate z, i.e. $z_{rms} = \sqrt{\langle z^2 \rangle}$.

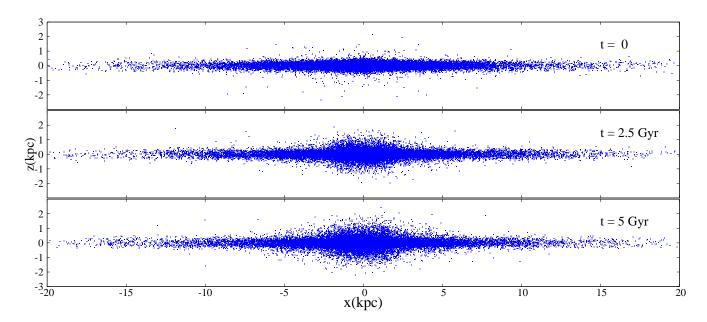


Figure 3. Edge on disks show the evolution of stellar orbits at three different times (0, 2.5 and 5 Gyr). The model corresponds to an Sc galaxy. The thickening of the disk due to the spiral arms presence is clear.

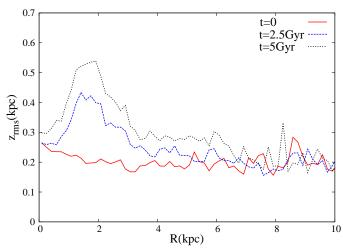


Figure 4. Disk thickness z_{rms} as a function of R for t=0, 2.5 Gyr and 5 Gyr.

Figure 4 shows the thickness as a function of R for the stellar disks in Figure 3.

From these first set of experiments, we conclude that the sharpest effect on the velocity dispersion, is present on the latest morphological types. It is worth mentioning here that, although we are separating the models in Sa, Sb and Sc galaxies, with strong gaps in between the different models in the initial scale height, the results on the disk heating driven by spiral arms presented here, are more general, i.e. the observed heating results significant in thinner disks, which, as a consequence, has implications on galaxy types, in this case, particularly on later types.

For the earliest type (Sa), the isolated effect of spiral arms corresponds to a maximum increment of 7% percent of the initial velocity dispersion, this considering the most massive and the largest pitch angles possible to produce plausible galactic models. Likewise, for

the intermediate galactic type (Sb), the isolated effect of spiral arms corresponds to a maximum of increment 20% percent of the initial velocity dispersion, again considering the most massive and the largest pitch angles possible to produce plausible galactic models. Finally, for the latest type (Sc), the isolated effect of spiral arms corresponds to a maximum of 62% percent of the initial velocity dispersion for this example, where we have not used the maximum plausible parameters for the spiral arms. When the maximum pitch angle and mass is employed, the percentage goes up to almost 90% of the initial velocity dispersion.

Since a visible effect in the vertical dispersion when spiral arms are included is considerably larger for the latest galactic types, compared with early and intermediate types, in the next sections we concentrate on a more detailed study of the disk thickening focusing only in the late type galaxies.

3.1.1. The pitch angle effect

The pitch angle is one of the most influential structural parameters that characterize spiral patterns. In this section a range of values is explored in order to quantify the dependence of the increment in the vertical velocity dispersion with pitch angle in the most affected galactic models, that are the latest types.

Figure 5 shows three plots of σ_z vs R, where the mass of the spiral arms is set to a constant for each plot and the pitch angle vary according to Table 1. Each plot has the initial dispersion curve $\sigma_z(R,t=0)$ and the dispersion after a 5 Gyr evolution $\sigma_z(R,t=5\,\mathrm{Gyr})$ for each pitch angle value.

From Figure 5, it is clear that regardless the mass of the spiral arms, the vertical velocity dispersion increases notably with the pitch angle. The less massive the spiral arms the smaller is their effect in general, as expected. Indeed, for spiral arms masses smaller that $\sim 1\%$ of the disk, the contribution of spiral arms to the dynamical heating becomes negligible.

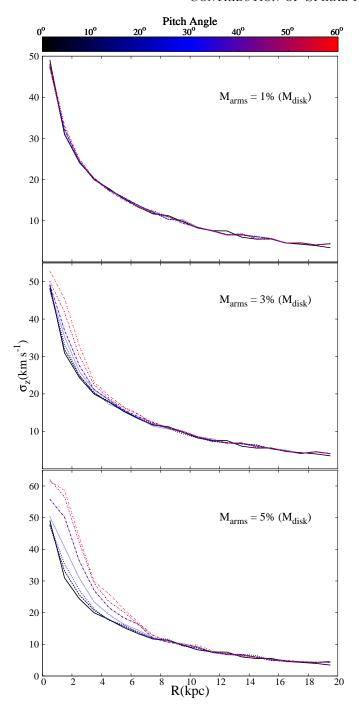


Figure 5. Final velocity dispersion after a 5 Gyr evolution as a function of radius for spiral arm masses of 1%, 3%, and 5% of the total disk mass.

3.1.2. The spiral arm mass effect

As it is shown in the previous section, the effect of the pitch angle can be significant to the disk thickening. It also results intuitively clear that this also scales with the mass of the spiral arms. To address this point, we produced several experiments condensed in Figure 6, that show the disk thickening dependence on the spiral arms mass and the pitch angle together. For this purpose, first we identified the radius R_{max} at which occurs the maximum difference between the final and initial vertical

velocity dispersion. We find that this occurs at approximately $R_{max}=1.5\,\mathrm{kpc}$ for this model. We then keep R constant at that value and plot $\Delta\sigma_z$ there as a function of the pitch angle. This will show us the tendency seen in the previous section. Now repeating this for the three spiral arms masses employed will show how $\Delta\sigma_z$ scales with this second parameter.

Figure 6 shows $\Delta \sigma_z$ as a function of the pitch angle for three different masses of the spiral arms. Here it is clear that both parameters, the pitch angle and the mass of the spiral arms, affect considerably the disk thickening effect driven by the spiral structure.

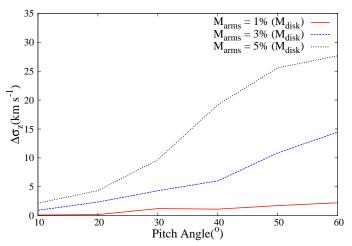


Figure 6. Difference in the vertical velocity dispersion $\Delta \sigma_z$ (at t=0 and t=5Gyr) vs the pitch angle, plotted for the three masses of the spiral arms, as a scaling factor.

We produce with these results an empirical functional relation between $\Delta \sigma_z$ and the Pitch Angle. The fit of data plotted in figure 6 is made by noting that $\Delta \sigma_z$, increases slowly at small angles, then the slope of the curve grows with the angle and flattens for the largest values of the pitch angle. This behavior could be interpreted as a saturation effect of $\Delta \sigma_z$ after a certain time, this time being shorter for higher angles and masses. The saturation effect is also seen in a σ - time relation (Seabroke & Gilmore 2007; Soubiran et al. 2008; Calberg et al. 1985), where the dispersion remains constant after $\sim 5 \, \text{Gyr}$. Based on this observation, a nice fit to the results would be a Boltzmann sigmoidal function which is characterized by displaying a progression from small beginnings that accelerates and approaches a climax over the independent variable. The Boltzmann sigmoidal function, for this particular case, is defined by

$$\Delta \sigma_z = A_2 + \frac{(A_1 - A_2)}{1 + exp((x - x_0)/d)}$$
 (10)

where: $x = \text{Pitch Angle } (^{o})$ $x_{0} = \text{center } (^{o})$ $d = \text{width } (^{o})$ $A_{1} = \text{initial } \Delta \sigma_{z} \text{ value } (\text{km s}^{-1})$ $A_{2} = \text{final } \Delta \sigma_{z} \text{ value } (\text{km s}^{-1})$ The center x_0 is the pitch angle at which $\Delta \sigma_z$ is halfway between A_1 and A_2 . The width d is related with the steepness of the curve, with a larger value denoting a shallow curve.

Figure 7 shows the fit of the sigmoidal function (Eq. 10) to the data. We see that this function reproduces well the behavior of $\Delta \sigma_z$ with the pitch angle for the three masses of spiral arms used in our simulations.

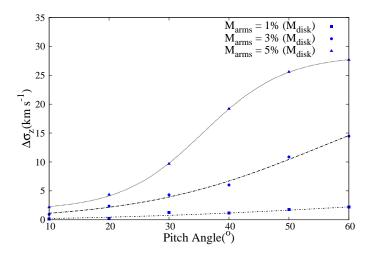


Figure 7. Fit of the $\Delta \sigma_z$ - pitch angle relation with the Boltzmann sigmoidal function for the three masses of the spiral arms.

Taking Eq. (10) as the functional form for the $\Delta \sigma_z$ -pitch angle relation, in Table 2, we summarize the parameters that describe the fits plotted in figure 7 for the three spiral arms masses.

Gradually Increasing the Mass of the Spiral Arms

As explained before, the spiral structure in our galaxy potential models is imposed and fully introduced since the starting point of the simulation. However, one might wonder if spurious effects (such as a drastic dispersion increase in the early stages of the simulation) are introduced with this method; also, in real galaxies the birth and death of spiral arms is most probable not a sudden process.

In order to explore these two scenarios, we prepared a set of representative simulations modifying the model in such a way that the arms are allowed to have a growing period until the total assigned mass is reached. For this set of simulations we started with an Sc galaxy with different combinations of values for the spiral arms mass and the pitch angle. We chose two radial positions and measured in there the evolution of σ_z with time as showed in Figure 8. In this figure the temporal evolution of σ_z for the sudden full mass arms is compared with a model with linear (1 Gyr period) growing mass. It is clear that there is a shift in the dispersion achieved at the end of the simulation, but most important, for both kinds of imposed spiral arms the velocity dispersion increases at roughly the same rate.

With this simple experiment we are not pretending to capture the great variety of processes that lead to the formation of a real spiral pattern, nor their timelapse of

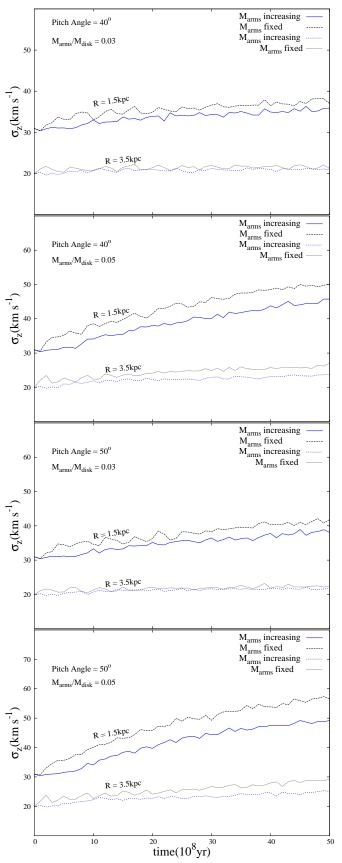


Figure 8. σ - t relation that shows, regardless the radial position, a continuous heating for both kind of imposed spiral arms: those that grow with time (blue lines) and those totally formed since the beginning (black lines).

$\mathbf{Table} 2$				
$\Delta\sigma_z$ -	Pitch	Angle	Fit	Details

M_{arms} (% M_{disk})	x_0 (°)	$d(^{o})$	$A_1 \; ({\rm km}{\rm s}^{-1})$	$A_2 \; ({\rm km}{\rm s}^{-1})$
1%	64.73	$24.05 \\ 14.95 \\ 6.82$	-0.33	5.32
3%	54.73		-0.057	24.84
5%	35.68		1.69	28.44

Note. — Parameters that combined with equation 10, describe the $\Delta \sigma_z$ - pitch angle relation. Center x_0 , width d, initial $\Delta \sigma_z$ value A_1 , and final $\Delta \sigma_z$ value A_2 . For the three spiral arms masses (in percentage of the disk mass M_{disk}).

full action, but this is still likely a better approximation than a sudden action of spiral arms. With this excercise we notice however that, for any radial position, the vertical dispersion is only shifted when using spiral arms that have a growing period. This do not suppose important differences with our previous simulations or results derived from them.

3.1.3. Varying the Angular Velocity of the Spiral Pattern

The vertical heating of the stellar disk produced by the spiral arms depends on the parameters of the nonaxisymmetric structure, particularly for the late galaxy types. By varying the pitch angle and the mass of the arms we have found a correlation between this parameters and the thickness of the stellar disk.

In this section, we study now the pattern speed effect on the disk vertical heating. For this purpose, we ran a set of simulations with different values of the spiral pattern for the latest types of galaxies: Sb and Sc, that are more clearly affected for the structural parameters of the arms. In Figure 9 we show first the evolution of the vertical velocity dispersion σ_z over time up to 5 Gyr for different values of the pattern speed, Ω , for an Sc galaxy. There seems to be a clear relation between the angular velocity and the dynamical heating. The velocity dispersion increases for slower rotating patterns.

Figures 10 and 11 summarize the results of the set of simulations when varying the pattern speed for Sb and Sc galaxies. The final stage of σ_z is shown across the entire disk for each one of the pattern speeds used. As expected, the final vertical velocity dispersion and disk thickness are larger for slower rotating arms, independently of the galaxy type. Smaller values of Ω allow the spiral arms to heat more efficiently the stellar disk, likely due to the minor relative angular velocity between the arms and the stars, this allows the stars to interact with the potential of the arms for longer periods of time.

Other studies link the heating of the stellar disk and the role of the pattern speed only to the resonant regions of the spirals (Lynden-Bell & Kalnajs 1972; De Simone et al. 2004), in contrast, in this study we find that the heating, radial and vertical, occurs along the entire length of the spiral arms.

On the other hand N-body simulations had shown to develop transient spiral structure that spans a range of pattern speeds (Sellwood & Binney 2002; Roskar et al. 2012), but as the arms are transient and is not possible to isolate its effect in N-body simulations, it results difficult to establish a dependence of the heating on the pattern speed.

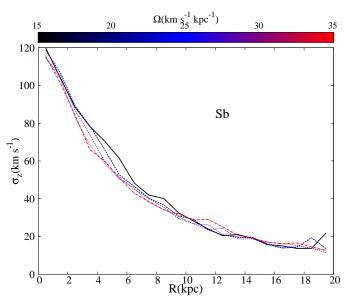


Figure 10. Final velocity dispersion after a 5 Gyr evolution for different spiral pattern angular speeds in an Sb galaxy.

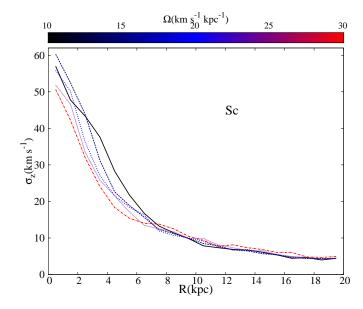


Figure 11. Final velocity dispersion after a 5 Gyr evolution for different spiral pattern angular speeds in an Sc galaxy.

The experiments and the model shown here allows us

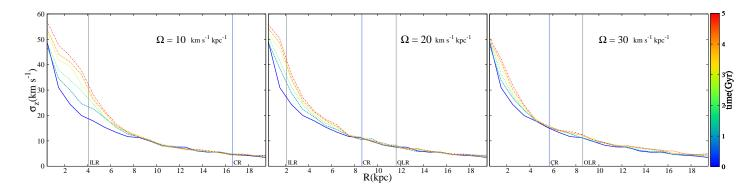


Figure 9. Time evolution of the vertical velocity dispersion for three different spiral pattern angular speeds in an Sc galaxy. This comparison shows that slower rotating spiral arms heat more efficiently the stellar disk.

to establish a relation between the vertical heating of the stellar disk and the pattern speed.

3.1.4. σ_z - Time Relation

It is already known that the age and velocity dispersion of stars are correlated. This has been established from observations in the solar neighbourhood as well as from numerical simulations (Holmberg et al. 2009; Roskar et al. 2013; 2014). The σ - t relation shows a smooth, general increase of the velocity dispersion with time and is best parametrized by a power law with exponents ranging between 0.2 - 0.5 (Gerssen & Shapiro Griffin 2012).

We explore the σ -t relation in our simulations to find out if the velocity dispersion in the stellar disk due to the spiral arms fits with a power law t^{α} and more important, to establish a range of values for α .

To measure the time evolution of σ_z in our simulations first we locate the radius R_{max} at which occurs the maximum increase in the vertical velocity dispersion. This radius is $R_{max}=1.5\,\mathrm{kpc}$ and is the same for all the simulations with the Sc galaxy, independently of the pitch angle or the mass of the spiral arms.

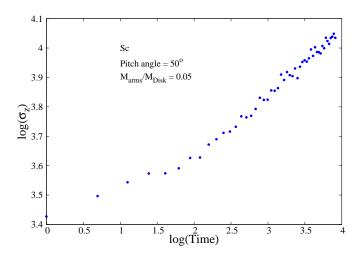


Figure 12. log-log plot of the time evolution of σ_z .

Since a log-log plot is useful to recognize a possible power law relationship, Figure 12 shows the log(t) -

 $log(\sigma_z)$ dependency. The most of the points fall on a straight line, this reveals a behavior of the form $\sigma_z \propto t^{\alpha}$.

Figure 13 shows the evolution of σ_z with time at $R=R_{max},~M_{arms}/M_{disk}=0.05$ and at different pitch angles: $20^{\circ},~30^{\circ},~40^{\circ}$ and 50° . The black line in each plot is the best fit of the data with a power law of the form $\sigma_z \propto t^{\alpha}$. We made the same analysis for a spiral arm mass of $M_{arms}/M_{disk}=0.03$, an interesting outcome is that the value of α is independent of the spiral arm mass. Different masses for the spiral arms will just change the proportionality constant in the relation $\sigma_z \propto t^{\alpha}$. Consequently, α depends only on the pitch angle, and for the angles used in our simulation α varies within the range 0.27-0.56 for Sc galaxies.

Although we have presented the time evolution of σ_z at $R=R_{max}$, it is possible to made the measure at any value of R. Figure 14 shows the same analysis at a different radial position, and this time corresponds to the half of the arm length, $R=4.2\,\mathrm{kpc}$. We notice that measuring the time evolution of σ_z at different radius give us the same power law behavior.

With a similar analysis for Sb galaxies, where $R_{max} = 2.5 \,\mathrm{kpc}$, we find again that a power law provides a nice fit to the data. Figure 15 shows the σ_z temporal evolution for pitch angles of 36^o and 45^o , and the best fits are reached with values for α of 0.32 and 0.37, respectively. Smaller angles than those give us plots with more scattered points where a power law fit is not straightforward to obtain, i.e., we are not able to establish the value of α for angles smaller than 36^o . For Sb galaxies we can only provide an upper bound for α of \sim 0.37.

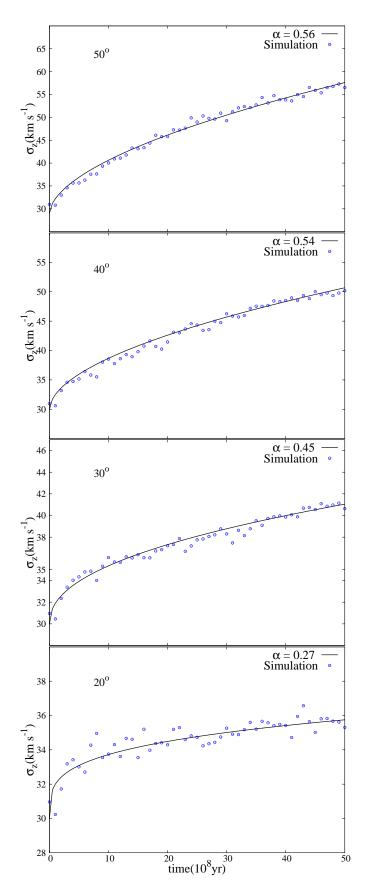


Figure 13. Temporal evolution of σ_z for a Sc galaxy. The panels correspond to four different pitch angles, from top to bottom: 50^o , 40^o , 30^o , and 20^o . The black lines show the best fit to the data for a relation of the form $\sigma_z \propto t^\alpha$.

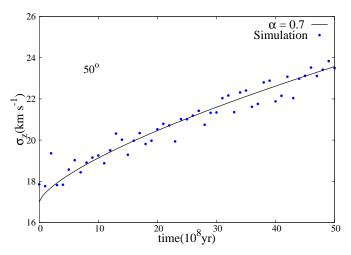


Figure 14. Time evolution of σ_z measured at half arm length for a Sc galaxy, 50^o pitch angles. The black line shows the best fit to the data for a relation of the form $\sigma_z \propto t^\alpha$.

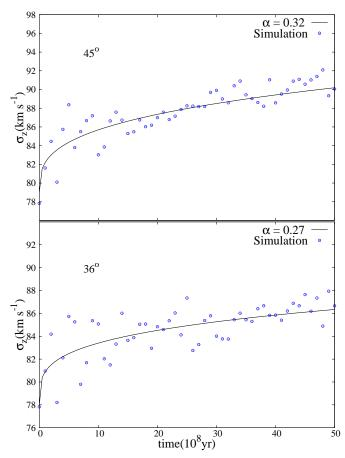


Figure 15. Temporal evolution of σ_z for an Sb galaxy. The panels correspond with two different pitch angles, 45^o (top) and 36^o (bottom). The black lines show the best fit to the data for a relation of the form $\sigma_z \propto t^\alpha$.

Considering that the pitch angles we are employing here represent the maximum plausible values of pitch angle and spiral arms mass for each type of galaxy, before chaos dominates, the values of α presented here would represent an upper bound for the contribution of the spiral arms to the vertical velocity dispersion of stars in each galaxy type.

3.1.5. The velocity ellipsoid

For the the dynamical evolution analysis of the stellar disk we applied a classic method derived from the distribution of the velocity dispersions. The axes of such distribution define the known as the "velocity ellipsoid", and this is characterized by the two axes ratios: σ_z/σ_R and σ_ϕ/σ_R .

The shape of the velocity ellipsoid seems to show a trend in σ_z/σ_R with the morphological type (Gerssen & Shapiro Griffin 2012). Given the three types of galaxies we are using in this work and the parameters given in Table 1 that defines them, we are able to measure the shape of the velocity ellipsoid and compare it with the morphological type. In Figure 16 we plot this ratio as measured at the final stage of our simulations. The value σ_z/σ_R decrease with galaxy type and the trend keeps with time.

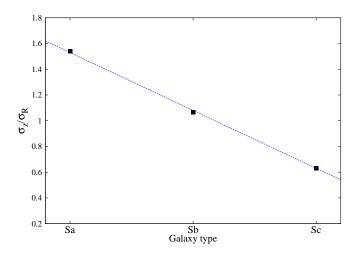


Figure 16. Velocity ellipsoid ratio σ_z/σ_R as a function of morphological galaxy type. The dashed line represents a linear regresion of the data.

In Figure 17 we follow the temporal evolution for the shape of the velocity ellipsoid. We see that for Sa and Sb galaxies σ_z is always greater than σ_R and the presence of spiral arms do not seem to alter this tendency. The initial fall in the curves indicates that although σ_z and σ_R both increase with time, σ_R does it in a greater proportion than σ_z , especially for late type galaxies. This heating in the R-direction is similar to that seen in Figure 2.

The shape of the velocity ellipsoid evolves towards lower values and settles down to be nearly constant and fluctuates around some equilibrium value, a behavior already noticed in other numerical work (Sellwood 2008).

Looking at the values of the plots in Figure 17, we see that the velocity dispersions ratio falls to half its initial value for Sa and Sb galaxies, with σ_z always greater than σ_R , but the final value of σ_z/σ_R falls lower than one for Sc galaxies. This indicates that the relative increase of σ_R for Sc galaxies is greater than that seen on Sa and

Sb galaxies. This means that the heating effect of the spiral arms in Sc galaxies, apart from being more notorious in the z-direction, is also greater in the R-direction compared to the other galaxy types.

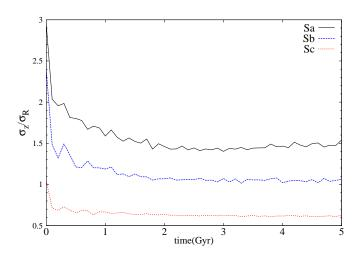


Figure 17. Velocity ellipsoid shape at 5 Gyr time evolution in our simulations for the three galaxy types simulated.

In previous sections we have shown that the vertical heating of the stellar disk strongly depends on the pitch angle of the spiral pattern. Consequently, the disk thickness in our simulations grows with the value of the pitch angle as seen in Figure 5 and equation 10. As showed in Jenkins & Binney (1990), where the ratio σ_z/σ_R depends on the spiral structure, here we are able to measure the shape of the velocity ellipsoid and its dependence on the pitch angle. Because the ratio of the velocity dispersion reaches a nearly constant value only after a certain period of time, under the influence of the spiral pattern (Figure 17), we computed the ratio σ_z/σ_R at the final stage in our simulations (5 Gyr) for several pitch angles, for the Sc galaxy. In Figure 18 we show how the shape of the velocity ellipsoid would be as a function of the pitch angle. It decreases first as the pitch angle grows but after a 40° angle it fluctuates around some constant value.

For small pitch angles ($<20^{o}$), the radial and vertical dispersions are nearly the same and this relation continues after 5 Gyr, despite the presence of the spiral pattern. This is because even when σ_z and σ_R increase with time, the grow rate is small in both directions compared with the initial dispersions. On the other hand, Figure 18 shows that for larger pitch angles, not only the increment in σ_z is considerable, as it is found in section 3.1.1, but the heating in the R-direction is remarkably, even greater than that in the z-direction. This is expected from a structure that rotates in the plane of the galaxy, but here we have found that it has a considerable effect in both, the radial and vertical directions, and variates sensibly with the parameters of the spiral pattern.

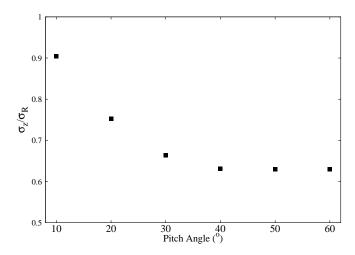


Figure 18. Velocity ellipsoid shape, measured after a 5 Gyr time evolution as a function of the pitch angle in an Sc galaxy.

3.1.6. Transient spiral arms

All results presented in the previous sections are obtained from simulations that assume long-lived spiral arms. However, it is a result from N-body simulations, that the spiral arms might rather be transient features in general (Sellwood 2011; Kawata et al. 2011).

In this section we present some experiments with transient spiral arms now, to quantify its effect in the vertical structure of the stellar disk and to study possible differences with our previous results. The adjustability of the galaxy models allows us to emulate transient and recurrent spiral arms by making them grow and disappear periodically. The lifetime of the spiral patterns is hard to determine in N-body simulations, and even in the cases where it can be determined with Fourier modes analysis, it is different for every simulation. We take two different periods for a simple experiment, one with 100 Myr and other with 500 Myr (Grand et al. 2014).

The simulations are made with an Sc galaxy model with a spiral arms pitch angle of 50° , $M_{arms}/M_{disk} = 0.05$, and two different lifetimes for the transient spiral arms. Figure 19 shows the vertical velocity dispersion σ_z as a function of R for the 5 Gyr evolution time with the transient spiral arms. Even with this kind of spiral pattern that is not always present in the disk, grows and disappear periodically, we can see that σ_z keeps increasing with time for both lifetimes used, as it does in our previous simulations with longer lasting spiral arms.

In Figure 20 we compare the final vertical velocity dispersion for both models of transient spirals against that obtained for non-transient spiral arms. The plots show only slight deviations between them, and not significative at all radii.

For a more detailed comparison we pick the radial zone at which the increase in vertical velocity dispersion is highest and plot the temporal evolution of σ_z for the transient and non-transient spiral arms and show it in Figure 21. Some slight differences are visible at the end of the simulation, and as this radial zone is where $\Delta\sigma_z$ is maximum, the differences are even smaller for the rest of the disk.

Despite the different nature of the three types of spiral

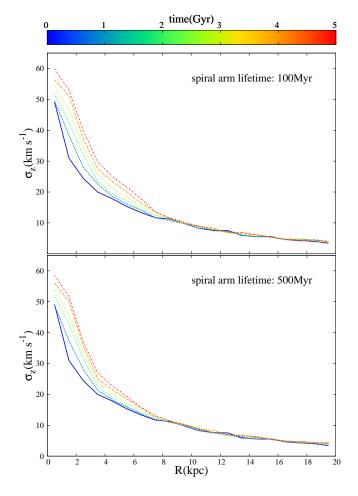


Figure 19. Vertical velocity dispersion as a function of R along 5 Gyr evolution time for transient spiral arms with lifetimes $100\,\mathrm{Myr}$ and $500\,\mathrm{Myr}$.

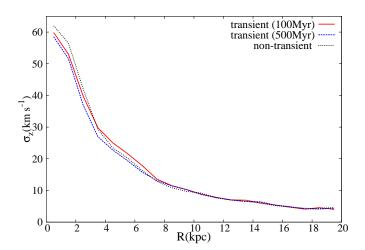


Figure 20. A comparison of σ_z after 5 Gyr for transient spiral arms, 100 Myr lifetime, 500 Myr lifetime, and non-transient spiral arms

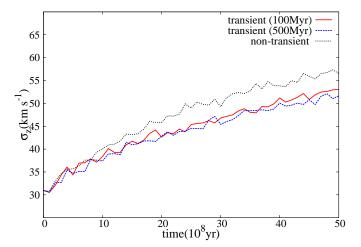


Figure 21. Comparing the time evolution of σ_z for transient spiral arms, 100 Myr lifetime, 500 Myr lifetime, and non-transient spiral arms.

arms simulated, the induced stellar dynamical behavior is similar. This is because the transient spiral arms, although not always present in the disk, are recurrent and form very quickly once the previous spiral pattern disappear as seen in N-body simulations, leaving the stars under an almost constant influence.

3.2. Plausible Origin of the Vertical Stellar Heating

Based on the set of experiments presented here, we conclude that a spiral structure can excite, considerably, velocities in the z-direction. Furthermore, we noticed that the physical mechanism causing the heating is different from simple resonant excitation. The spiral pattern induces chaotic behavior not linked necessarily to resonances, but rather to direct scattering of disk stars, which leads to an increase of the velocity dispersion.

In order to produce evidence to support this gravitational scattering interpretation, we performed the following analysis. For an Sc galaxy with spiral mass $M_{arms} = 0.05 \ M_{disk}$ and a pitch angle of 50°, we took a sample of 458 particles that at the end of the simulation are part of the hot component (i.e. particles that experienced a significant increase in their velocity dispersion). By tracing back the initial positions, we reconstruct the orbit of each particle. To classify the orbits and distinguish them as regular or irregular, we implemented a known spectral method by Carpintero & Aguilar (1998). The method is able also to identify loop, box, and other resonant orbits. The results are presented in Figure 22.

This analysis shows that the orbital sample is completely dominated by irregular orbits, with no evidence of resonances from any kind. In this way we interpret the vertical heating as caused by gravitational scattering of stars by spiral arms, as already has been pointed out in other studies (Fujii et al. 2011).

3.3. The case of the Milky Way

Probably, the hardest case to study due to the plethora of information available, sometimes contradictory, some other model or observations dependent, is the Milky Way Galaxy. The existence of different types of disks, or different types or vertical structures (the old and young thin disks, and the thick disk) has been known but not

for long. What are the mechanisms that produce the heating of stellar orbits into the thick disk?, what is the relative importance of each one? is this present in all galaxies? the mechanisms that affect radially the disks are effective in the vertical component?

A lot of the finest work on mechanisms to heat dynamically the disk has been done in the plane with steady two-dimensional potential models studying fundamental physical phenomena such as the radial migration. Regarding the vertical structure, this is a subject that started several decades ago to be of interest in astrophysics. Only recently, thanks to the calculation power of the new generation of supercomputers, we have been able to produce more realistic and detailed simulations with test particles in steady potentials and with alive models with improved resolution, all to study with unprecedent details the dynamics of the Galactic disk.

In this section, as a preliminary application to a specific galaxy, we have constructed a detailed density distribution, based model of the Milky Way Galaxy that includes spiral arms, with the purpose of exploring their isolated effect on the heating to the disk, and its participation in the process of production of the thick disk. We compare our results with other recent work dedicated to Milky-Way-like potentials (Faure et al. 2014). Additionally, the experiments presented in this section for the Milky Way, include one more experiment incorporating to the calculations the Galactic bar. We are not pretending this to be an extensive study of the Milky Way Galaxy, but rather a modest first approximation and preliminary results of only the vertical heating effects by spiral arms and bar on a detailed model of the Galaxy, in consequence it is important to mention, we are not including all the relevant references to this problem. In an ongoing work, we will provide a work fully dedicated to the Milky Way Galaxy in this context and the relevant references.

The parameters of the galactic models employed here, allow us to model different morphological types and different spiral arms classes by changing the pitch angle, the mass or even making them transient. In this section, we produce observationally motivated models of the Milky Way galaxy and study the response of the stellar disk to the spiral arms. The parameters that describe the components that compose the axisymmetric background potential, are constrained by recent estimates of the galactic rotation curve. We adopt a pitch angle of 15.5° for the spiral arms, a mass $M_{arm}/M_{disk} = 0.03$, and an initial time of 0.5 Gyr to increase up to their full mass the spiral arms. For the first simulation presented for the Milky Way, we do not include a bar in order to try to isolate the influence of the spiral pattern in the stellar disk (and to compare with other similar work).

Figure 23 (top panel) shows the initial and final vertical velocity dispersion after a 5 Gyr evolution for the Milky-Way-like model (halo, disk, bulge and spiral arms). As seen for the case of early type galaxies (i.e. small pitch angles and spiral arm masses), the change in velocity dispersion is small. Indeed, although the effect is not negligible, in the Milky-Way-like model experiment, with a pitch angle of 15.5° and a mass $M_{arm}/M_{disk}=0.03$, the spiral arms are not capable to heat the stellar disk. In Figure 23 (bottom panel) we plot the difference between σ_z initial and final, and show that the main heating is

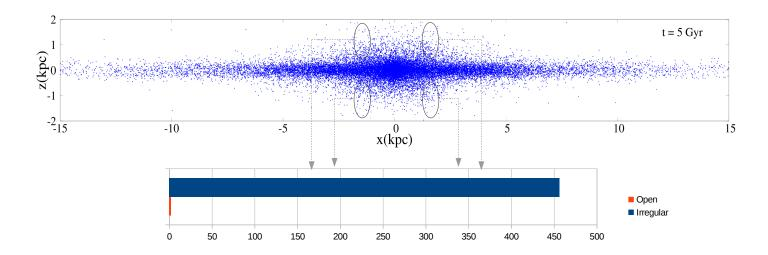


Figure 22. Orbital classification on the disk particles that experienced a significant increase in their velocity dispersion. The histogram shows that the orbital sample is dominated by irregular orbits.

Table 3Parameters for the Milky Way Model

Parameter	Value	Reference
	Axisymmetric Component	s
R_0	8.5 kpc	1
Θ_0	220 km s^{-1}	1
M_B	$1.41 \times 10^{10} \ {\rm M}_{\odot}$	1
M_D	$8.56 \times 10^{10} \ {\rm M_{\odot}}$	1
M_H	$80.02 \times 10^{10} \ \mathrm{M_{\odot}}^{-1}$	1
Disk scale-length	$2.5\mathrm{kpc}$	2
b ₁ ²	$0.3873~\mathrm{kpc}$	1
a ₂ ²	5.3178 kpc	1
b ₂ ²	$0.2500 \; \mathrm{kpc}$	1
a ₃ ²	$12 \mathrm{~kpc}$	1
	Spiral Arms	
locus	Logarithmic	3
arms number	2	4,5
pitch angle	15.5°	4
M_{sp}/M_D	3%	
scale-length	$2.5~\mathrm{kpc}$	disk based
Patter speed (Ω_{sp})	$-20 \text{ km s}^{-1} \text{ kpc}^{-1}$	6
inner limit	3.3 kpc	based on ILR
outer limit	$12 \mathrm{~kpc}$	based on CR
	Triaxial Bar	
major axis	3.5 kpc	2, 7
Scale length	1.7, 0.64, 0.44 kpc	2
Axial ratio	0.64/1.7, 0.44/1.7	
Mass	$1.41 \times 10^{10} \ {\rm M}_{\odot}$	
Pattern speed (Ω_B)	$50 \text{ km s}^{-1} \text{ kpc}^{-1}$	6

References. — (1)Allen & Santillán 1991. (2) Freudenreich 1998. (3) Seigar & James 1998; Seigar et al. 2006. (4) Drimmel et al. 2000. (5) Grosbøl et al. 2002; Churchwell et al. 2009; Elmegreen & Elmegreen 2014. (6) Gerhard 2011. (7) Binney et al. 1997; Bissantz & Gerhard 2002.

 $^{^{1}}$ Up to 100 kpc halo radius. 2 b₁, a₂, b₂, and a₃ are scale lengths.

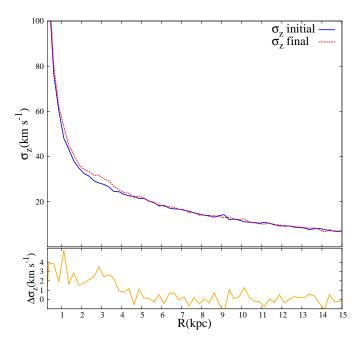


Figure 23. Effect of the Milky-Way-like Spiral Arms in the dynamical heating of the disk. Top: Initial and final vertical velocity dispersions after 5 Gyr evolution. Bottom: $\Delta \sigma_z$ (final-initial). The vertical heating is minimum over a small radial region.

produced in the innermost region of the disk.

With this experiment we conclude that the vertical heating that spiral arms are able to produce in our Milky-Way-like Galaxy model is minimum and it is located in a small radial region. This result represents a different one compared to that of Faure et al. (2014), that find some important effect on the vertical heating due to the spiral arms. To try to account for the origin of this discrepancy, further studies will be performed in a future work.

In a second experiment, we have also included a known mechanism that exerts strong secular radial and vertical evolution on galactic disks, the central bar. Although the present work is advocated to the study of the effect of the spiral arms on stellar disks vertical heating, we have produced a careful experiment for the Milky Way Galaxy to explore to what extent the central bar can contribute to the vertical heating. In an ongoing paper we study in detail the vertical heating produced by the full galactic model of the Milky Way, here we present some preliminary results of this study.

We ran a simulation with the parameters representative of the Milky Way Galaxy, given on Table 3. Figure 24 shows the initial and final vertical velocity dispersion σ_z across the stellar disk. Although the two nonaxisymmetric structures are present in the simulation, by comparing Figures 23 and 24, there is no doubt that the heating seen in the second one is produced by the galactic bar, and that the only affected region seems to be the central part (similar results were obtained by (Saha, Tseng & Taam 2010)).

The effect of the galactic bar on the vertical velocity dispersion is considerably, with an increase in σ_z up to $16 \,\mathrm{km}\,\mathrm{s}^{-1}$, mostly in the inner 6 kpc of the disk.

4. CONCLUSIONS

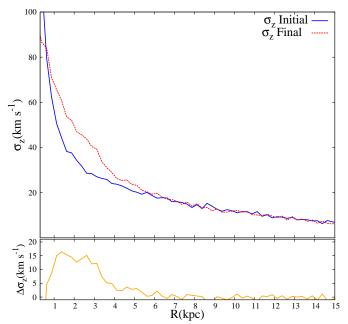


Figure 24. Effect of the Milky Way Spiral Arms + Bar model on the vertical disk Heating. Top: Initial and final vertical velocity dispersions after 5 Gyr evolution. Bottom: $\Delta \sigma_z$ (final-initial). The vertical heating is appreciable, with an increment up to $16 \, \mathrm{km \, s^{-1}}$ in the inner region of the disk.

With the use of detailed models for spiral galaxies, we produce an extensive study of disks vertical heating. The models include an axisymmetric component (bulge, massive halo and disk) plus a density based three dimensional potential for the spiral arms, orbitally tested for self-consistency.

The main outcome of this study is that the spiral structure is capable to excite moderate to high dispersion velocities in the z-direction inducing a relation between stellar age and σ_z in all spirals except the earliest types. Although rather small, this mechanism works for the Milky Way Galaxy, assuming the parameters for the spiral arms known to this day. Consequently, by isolating the effect of the spiral arms on the vertical velocity dispersion of the stellar disk, we can conclude that spiral arms have the capability to contribute to the heating mechanism that gives raise to thick disks in spiral galaxies, from intermediate to late morphological types.

Therefore, the thickness of the stellar disk driven by the spiral arms go from negligible to very important, depending on the characteristics of the spiral pattern such as mass, pitch angle and angular speed along with the morphological galaxy type. By covering a whole set of values for this parameters in the test particle simulations we conclude that:

• The relative increase in vertical velocity dispersion is a function of the morphological type, being smaller for early type galaxies (Sa type in the Hubble scheme) and larger from intermediate to late type galaxies. Although for the sake of clarity, we present our results by separating the models in approximately average Sa, Sb and Sc galaxy types, we are aware that strong gaps are in between the different models in the initial scale height. The

results on the disk heating driven by spiral arms presented here, are therefore more general, i.e. the observed heating is considerably more significant in thinner disks, which, as a consequence, has implications on galaxy types, in this case, particularly on later types.

- Two distinctive characteristics of the spiral arms are the mass and the pitch angle. By varying this parameters one at the time, within the permitted values, we found that they play equally important roles in the vertical heating of the stellar disk. As expected, massive arms and/or large pitch angles are responsible for the most prominent disk thickness found in our simulations.
- The other dynamical parameter characteristic of the spiral arms, is the pattern speed Ω . When varying this value, we found that the vertical heating induced by the spiral pattern is greater for slow rotating arms and decrease for those that rotate faster. Smaller values of Ω allow the spiral arms to interact more effectively with the stars, and heat more efficiently the stellar disk, independently of galaxy type.
- By measuring the time evolution of σ_z in our simulations, we found that the vertical heating induced by the spiral arms follows a power law $\sigma_z \propto t^{\alpha}$, as seen from observations in the solar neighbourhood and other numerical simulations. An interesting result is that the value of α depends only on the pitch angle and not on the mass of the arms.
- The ratio σ_z/σ_R , that defines the shape of the velocity ellipsoid, shows a clear trend with the morphological type that remains during the temporal evolution. The values of this ratio across the entire simulations show that the heating in the R-direction is remarkable, always greater that in the z-direction for the three galaxy types. This is expected from a structure that rotates in the plane of the galaxy, but here we have found that it has a considerably effect in both, the radial and vertical directions. Consequently, the spiral arms are key to determine the shape of the velocity ellipsoid.
- Although in this work we cover the general properties of normal spiral galaxies, we took advantage of the adjustability of our model to represent the gravitational potential of the Milky Way Galaxy. Analysing the change in velocity dispersion induced by the nonaxisymmetric structures of the Galaxy we found that: the galactic spiral arms are not capable to induce an important thickness in the stellar disk, the increase in vertical velocity dispersion is small, therefore, from this study we conclude that the spiral arms play no role in producing a thick disk. If we add the galactic bar on the other hand, the vertical velocity dispersion increase considerably, mostly within the region covered by the bar. This means that for the Milky Way, the bar is an important heating mechanism that should be considered in calculations, but mostly in the inner region of the disk.

We thank Octavio Valenzuela for enlightening discussions. We thank the anonymous referee for an excellent review that helped to improve this work. We thank PAPIIT through grant UNAM/DGAPA IN114114. CONACyT México under grants CB-2009-01, no. 132400, CB-2011, no. 166212. The authors acknowledge to CGSTIC at CINVESTAV for providing HPC resources on the Hybrid Cluster Supercomputer "Xiuhcoatl". LAMM is supported by a CONACYT scholarship. APV acknowledges the the postdoctoral Fellowship of DGAPA-UNAM, Mexico.

REFERENCES

Allen, C. & Santillán, A. 1991, Rev. Mexicana Astron. Astrofis., 22, 256

Antoja, T., Helmi, A., Figueras, F., & Romero-Gómez, M. 2012, European Physical Journal Web of Conferences, 19, 5002

Antoja, T., Valenzuela, O., Pichardo, B., et al. 2009, ApJL, 700, L78

Barbanis, B., & Woltjer, L. 1967, ApJ, 150, 461

Bensby, T., Alves-Brito, A., Oey, M. S., Yong, D., and Meléndez, J., 2011, ApJ 735, L46

Benson, A. J., Lacey, C. G., Frenk, C. S., Baugh, C. M., & Cole, S. 2004, MNRAS, 351, 1215

Binney, J., Gerhard, O., & Spergel, D. 1997, MNRAS, 288, 365 Binney, J., Dehnen, W., & Bertelli, G. 2000, MNRAS, 318, 658 Bissantz, N., & Gerhard, O. 2002, MNRAS, 330, 591

Block, D. L., Bournaud, F., Combes, F., Puerari, I.& Buta, R. 2002, A&A, 394, L35

Brosche, P. 1971, A&A, 13, 293

Carlberg R. G., Dawson P. C., Hsu T., Vandenberg D. A., 1985, ApJ, 294, 674

Carlberg, R. G. 1987, ApJ, 322, 59

Carpintero, D. D., & Aguilar, L. A. 1998, MNRAS, 298, 1 Chereul, E., Creze, M., & Bienayme, O. 1998, A&A, 340, 384

Chereul, E., Crézé, M., & Bienaymé, O. 1999, A&AS, 135, 5 Churchwell, E., Babler, B. L., Meade, M. R., et al. 2009, PASP,

Churchwell, E., Babler, B. L., Meade, M. R., et al. 2009, PASP, 121, 213

Comerón, S., Elmegreen, B. G., Knapen, J. H., et al. 2011, ApJ, 741, 28

Dehnen, W. 1998, AJ, 115, 2384

De Simone R., Wu X., Tremaine S., 2004, MNRAS, 350, 627 Di Matteo, P., Lehnert, M. D., Qu, Y., & van Driel, W. 2011, A&A, 525, L3

Drimmel, R. 2000, A&A, 358, L13

Eggen, O. J. 1959, The Observatory, 79, 143

Eggen, O. J. 1977, ApJ, 215, 812

Eggen, O. J. 1990, AJ, 100, 1159

Eggen, O. J. 1996a, AJ, 111, 1615

Eggen, O. J. 1996b, AJ, 112, 1595

Egusa, F., Kohno, K., Sofue, Y., Nakanishi, H., & Komugi, S. 2009, ApJ, 697, 1870

Elmegreen, D. M., & Elmegreen, B. G. 2014, ApJ, 781, 11 Famaey, B., Jorissen, A., Luri, X., et al. 2005, A&A, 430, 165

Famaey, B., Siebert, A., & Jorissen, A. 2008, A&A, 483, 453 Fathi, K., Beckman, J. E., Piñol-Ferrer, N., Hernández, O.,

Martínez-Valpuesta, I. & Carignan, C. 2009, ApJ, 704, 1657
Faure, C., Siebert, A., & Famaey, B. 2014, MNRAS, 440, 2564
Font, A. S., Navarro, J. F., Stadel, J., & Quinn, T. 2001, ApJL, 563, L1

Freudenreich, H. T. 1998, ApJ, 492, 495

Fuchs, B. 2001, MNRAS, 325, 1637

Fujii M. S., Baba J., Saitoh T. R., Makino J., Kokubo E., Wada K., 2011, ApJ, 730, 109

Gerhard, O. 2011, Memorie della Societa Astronomica Italiana Supplementi, 18, 185

Gerssen, J., & Shapiro Griffin, K. 2012, MNRAS, 423, 2726 Grand R. J. J., Kawata D., & Cropper M., 2012, MNRAS, 421, 1529

Grand R.J.J., Kawata D., & Cropper, M., 2014, arXiv:1310.2952v2

Grosbøl P., Pompei E., & Patsis, P., 2002, ASPCS, 275, 305 Grosbøl, P., & Dottori, H. 2009, A&A, 499, L21 Grosbøl, P. J., & Patsis, P. A. 1998, A&A, 336, 840 Hänninen, J., & Flynn, C. 2002, MNRAS, 337, 731

Hernquist L., 1993, ApJS, 86, 389

Holmberg J., Nordstrom B., & Andersen J., 2009, A&A, 501, 941

Huang, S., & Carlberg, R. G. 1997, ApJ, 480, 503 Inoue, S., & Saitoh, T. R. 2014, MNRAS, 441, 243

Jenkins A., & Binney J., 1990, MNRAS, 245, 305

Kennicutt, R., 1981, AJ, 86, 1847

Kawata, D., Grand, R.J.J., & Cropper, M., 2011, arXiv:1110.3824v1

Kawata D., Hunt J. A. S., Grand R. J. J., Pasetto S., Cropper M., 2014, MNRAS, 443, 2757

Kroupa, P. 2002, MNRAS, 330, 707

Lacey, C. G. 1984, MNRAS, 208, 687

Lacey, C. G., & Ostriker, J. P. 1985, ApJ, 299, 633

Lépine, J. R. D., Cruz, P., Scarano, S., Jr., et al. 2011, MNRAS, 417, 698

Lin, C.C., Shu, & F.H. 1964. ApJ140, 646-655.

Lin C. C., Yuan C., Shu F. H., 1969, ApJ, 155, 721 Lynden-Bell D., Kalnajs A. J., 1972, MNRAS, 157, 1

Ma, Jhun, Zhao, Jun-liang, Zhang, Fei-peng, & Peng, Qiu-he 2000, Chinese Astronomy and Astrophysics, 24, 435

Majewski, S. R. 1994, ApJL, 431, L17

Majewski, S. R., Munn, J. A., & Hawley, S. L. 1996, ApJ, 459,

Martig M., Minchev I., Flynn C., 2014, MNRAS, 443, 2452

Minchev I., Quillen A. C., 2006, MNRAS, 368, 623

Minchev I., Famaey B., Quillen A. C., Dehnen W., Martig M., Siebert A., 2012, A&A, 548, 127

Miyamoyo, M., & Nagai, R., 1975, Pub. Astr. Soc. Japan, 27, 533 Patsis, P. A., Contopoulos, G. & Grosbøl P., 1991, A & A, 243,

Pérez-Villegas, A., Pichardo, B., Moreno, E., Peimbert, A., & Velázquez, H. M. 2012, ApJL, 745, L14

Pérez-Villegas, A., Pichardo, B., & Moreno, E. 2013, ApJ, 772, 91 Pichardo, B., Martos, M., Moreno, E. & Espresate, J., 2003, ApJ, 582, 230

Pichardo, B., Martos, M., & Moreno, E. 2004, ApJ, 609, 144 Pizagno, J., Prada, F., Weinberg, D. H., Rix, H. W., Harbeck, D., Grebel, E. K., Bell, E. F., Brinkmann, J., Holtzman, J. & West, A. 2005, ApJ, 633, 844

Pompéia, L., Masseron, T., Famaey, B., et al. 2011, MNRAS, 415,

Proctor, R. A. 1869, London, J. Browning, 1869.

Quillen, A. C., Dougherty, J., Bagley, M. B., Minchev, I., & Comparetta, J. 2011, MNRAS, 417, 762

Quinn, P. J., Hernquist, L., & Fullagar, D. P. 1993, ApJ, 403, 74 Roman, N. G. 1949, ApJ, 110, 205

Roskar R., Debattista V. P., Quinn T. R., Wadsley J., 2012, MNRAS, 426, 2089

Roskar R., Debattista V. P., & Loebman S. R., 2013, MNRAS, 433, 976

Roberts, W.W., Jr., Huntley, J. M., & van Albada, G. D., 1979, ApJ, 233, 67

Saha K., Tseng Y.-H., Taam R. E., 2010, ApJ, 721, 1878

Scannapieco C., White S. D. M., Springel V., Tissera P. B., 2011, MNRAS, 417, 154 Seabroke G. M., Gilmore G., 2007, MNRAS, 380, 1348

Seigar, M. S., & James, P. A. 1998, MNRAS, 299, 685

Seigar, M. S., Bullock, J. S., Barth, A. J., & Ho, L. C. 2006, ApJ, 645, 1012

Sellwood, J. A., & Carlberg, R. G. 1984, ApJ, 282, 61

Sellwood J. A., Binney J. J., 2002, MNRAS, 336, 785 Sellwood J. A., 2008, in J. G. Funes & E. M. Corsini ed., Formation and Evolution of Galaxy Disks Vol. 396 of Astronomical Society of the Pacific Conference Series,

Dynamical Evolution of Disk Galaxies. p. 241

J.A. Sellwood, 2011, MNRAS 410, 1637 Sellwood, J. A. 2013, ApJL, 769, L24

Snaith, O. N., Haywood, M., Di Matteo, P., et al. 2014, ApJ, 781, L31

Soderblom, D. R., & Mayor, M. 1993, AJ, 105, 226

Sofue, Y. & Rubin, V. 2001, ARA&A, 39, 137

Soubiran C., Bienaymé O., Mishenina T. V., Kovtyukh V. V., 2008, A&A, 480, 91

Spitzer, L., Jr., & Schwarzschild, M. 1951, ApJ, 114, 385 Toomre, A., 1964, ApJ., 139, 1217

van der Kruit, P. C., & Searle, L. 1981, A&A, 95, 116

Vande Putte, D., Cropper, M., & Ferreras, I. 2009, MNRAS, 397,

Velazquez, H., & White, S. D. M. 1999, MNRAS, 304, 254

Villalobos, A., & Helmi, A. 2008, MNRAS, 391, 1806 Villumsen, J. V. 1983, ApJ, 274, 632

Weinzirl, T., Jogee, S., Khochfar, S., Burket, A. & Kormendy, J. 2009, ApJ, 696, 411

Wielen, R. 1977, A&A, 60, 263

Wilson, R. E., Boss, B., & Raymond, H. 1923, AJ, 35, 26

Yoachim, P., & Dalcanton, J. J. 2006, AJ, 131, 226

Yoachim, P., & Dalcanton, J. J. 2008, ApJ, 682, 1004